Case Studies in Thermal Engineering 34 (2022) 102003

Contents lists available at ScienceDirect

Case Studies in Thermal Engineering

journal homepage: www.elsevier.com/locate/csite

A new fusion-edge sealed vacuum for concentrated photovoltaic/thermal solar collector in comparison to a conventional system

Essam M. Abo-Zahhad [a,b,*], Saim Memon [c,d], Ali Radwan [e,f], Mohamed R. Elmarghany [f,g], Asmaa Khater [f,g], Chaouki Ghenai [a,e], O. Abdelrehim [f,g]

[a] Renewable Energy and Energy Efficiency Research Group, Sustainable Energy and Power Systems Research Centre, Research Institute for Sciences and Engineering (RISE), University of Sharjah, P.O. Box 27272, Sharjah, United Arab Emirates
[b] Mechanical Power Engineering Department, Faculty of Energy Engineering, Aswan University, Aswan, 81528, Egypt
[c] Solar Thermal Vacuum Engineering Research Group, London Centre for Energy Engineering, School of Engineering, London South Bank University, 103 Borough Road, London, SE1 0AA, UK
[d] Department of Engineering and Technology, School of Computing and Engineering, University of Huddersfield, Huddersfield, West Yorkshire, HD1 3DR, UK
[e] Department of Sustainable and Renewable Energy Engineering, College of Engineering, University of Sharjah, Sharjah, P.O. Box 27272, Sharjah, United Arab Emirates
[f] Mechanical Power Engineering Department, Faculty of Engineering, Mansoura University, El Mansoura, 35516, Egypt
[g] Mansoura University Nanotechnology Center, Mansoura University, El-Mansoura, 35516, Egypt

GRAPHICAL ABSTRACT

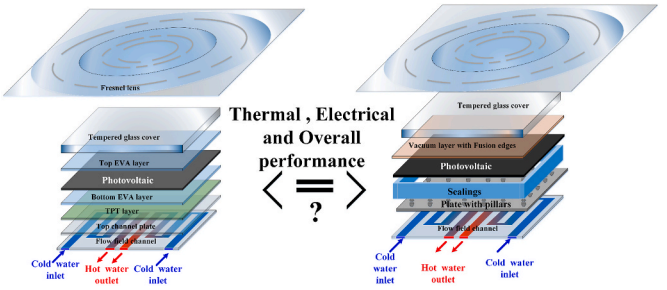

ARTICLE INFO

Keywords:
Vacuum insulation
Concentrated photovoltaic/thermal
Thermal analysis

ABSTRACT

Any heat harvesting system experiences high heat loss to the ambient. Hence, using matured insulation such as vacuum insulation to control any thermal heat leakage is highly required. In the current research investigation, a novel hybrid new fusion-edge sealed vacuum concentrated so-called VCPV/T system. The new design of a vacuum insulated layer is employed to reduce the

* Corresponding author. Renewable Energy and Energy Efficiency Research Group, Sustainable Energy and Power Systems Research Centre, Research Institute for Sciences and Engineering (RISE), University of Sharjah, P.O. Box 27272, Sharjah, United Arab Emirates./
E-mail addresses: Essam_Mohamed@aswu.edu.eg, emohamed@sharjah.ac.ae (E.M. Abo-Zahhad).

https://doi.org/10.1016/j.csite.2022.102003
Received 29 January 2022; Received in revised form 28 March 2022; Accepted 3 April 2022
Available online 14 April 2022

Exergy analysis
Electrical analysis

thermal losses and improve the overall electrical, thermal, and exergy performance of a concentrated photovoltaic solar thermal collector (CPV/T). A comprehensive 3D conjugate heat transfer model is developed, validated with mesh independent tests for both CPV/T and VCPV/T at *Re* of 75 to achieve the higher precision of results in numerical simulations. The results show in the new VCPV/T the percentage rise in the maximum cell temperature between both systems achieved to be 1.0%, 1.7%, and 2.16% at three different concentration ratios (*CR*) of 1, 2, and 3, respectively. The results of VCPV/T implicate a sensible enhancement in the overall performance compared to the conventional CPV/. For, $CR = 3$, the maximum thermal, electrical, and total exergy predicted to be 144.5 W, 33 W, and 177.6 W all around 13:00 h for new VCPV/T systems, respectively. At $CR = 3$, about 14% and 10.7% enhancement in thermal and total exergy, respectively.

1. Introduction

Solar thermal energy collectors are the most abundant energy conversion and utilization resource because they can be used in both direct and indirect modes for primarily hot water supply in buildings. The total global solar thermal capacity in operation in 2019 was 479 GWth, with a projected annual energy production of 389 TWh, representing global energy savings of 41.9 Mtoe and a CO_2 reduction of approximately 135.1 million tons [1]. Notably, the global capacity of both unglazed and glazed solar hot water collectors in operation rose from 62 GWth/51 TWh (89 million m^2) in 2000 to 479 GWth/389 TWh (684 million m^2) in 2019. The integration of solar thermal collectors with photovoltaic (PV) panels (PV/T) for hot water supply and electrical energy generation has been widely investigated [2]. Because of the improved heat transfer provided by evacuated tubes, evacuated tube solar hot water collectors accounted for 70.4% of all collectors installed globally in 2018 [1]. Shahzad et al. [3] highlighted the importance of the energy-water-environment nexus to achieving the COP21 goal and maintaining environment temperature rise below 2 °C. The authors showed the records of CO2 emission which unfortunately confirms that two-thirds share of it has already been used and the residual will be exhausted by 2050.

Solar power costs can be reduced by focusing sunlight or concentrated solar irradiation in PV cells, which effectively minimize costly rooftop PV areas, using inexpensive concentrating mirrors such as Fresnel lenses. In the concentrated PV/T (CPV/T) systems, the concentration optics are used to focus and direct incoming solar irradiation into the lower area of the PV receiver compared with nonconcentrated systems [4]. The range of increase in thermal and electrical efficiencies expands with increasing solar concentration ratios (CR) values.

The CPV/T arrangements provide additional electrical and thermal energy generation by allowing the effective use of rooftop spaces and the reduction of solar PV system's capacity and area. However, the main PV/T issue, particularly in the CPV/T systems, is the significant increase in PV cell temperature, necessitating a more powerful thermal management system. This is because Si-based PV efficiency reduces by approximately 0.4%–0.6% per 1 K temperature increase [5]. Additionally, the heat absorbed by the absorber

Table 1
Limitations and key strengths of cooling method within the PV/T system [15].

Cooling system working fluid	Advantage and strength points	Challenges and limitations
Free air	• Straightforward, cost effective, extremely reliable, and quiet operation • Passive operation	• Restricted heat transfer levels, dependent relative on the area and ambient conditions • Possibility of dust accumulation problems
Liquid immersion	• Normal heat transfer capacity with the passive operation • Decreases optical losses from reflection and dust accumulation	• Enduring degradation, decay, leak, and salt scaling
Forced air	• Above-average heat transfer capacity than free air • Probable reuse of waste heat and warmed air	• High cost of manufacturing and maintenance • Heat transfer rates are limited by air • Possibility of dust accumulation problems
Liquid film or spray	• Cleaning the front surface of the PV and reducing optical losses • Probable reuse of waste heat and hot water	• Large surface areas are needed • Water cannot be recycled/no close cycle • High cost of manufacturing and maintenance
Jet impingement	• Ability to cool down high heat flux densities • Possibility for restricted space and compact systems	• High cost of manufacturing and maintenance • Temperature maldistribution, thermal gradient, and high nonuniformity degree
Microchannel	• Ability to cool down high heat flux densities with a compact package • Minimal pumping requirements could achieve with proper design • Possibility of reduction of thermal resistances and stresses, with direct fabrication	• High cost of manufacturing and maintenance • Temperature maldistribution, thermal gradient, and high nonuniformity degree • Manufacturing of complex microfluid devices needs high technology

plate must be quickly transferred to the working fluids to avoid system overheating [6].

PV/T collectors have been a prominent research topic over the past three decades. This is due to difficulties in the thermal management or cooling of PV cells with the liquid or gas media in the PV/T [7]. For example, air and water glass-covered collectors were explored first [8] but uncovered PV/T collectors were quickly considered by many researchers [8,9]. A wide range of working fluids have recently been studied, including ethylene glycol [10], oil [11], hybrid ethylene glycol/phase change material [12], hybrid water and air [13], and nanofluids [14].

N. Gilmore et al. summarized the limitations and key strengths of the cooling method within the PV/T system [15] in the Table 1.

The extensive efforts in the literature revealed a significant improvement in PV/T performance in terms of electrical and thermal efficiencies [8]. However, one may argue that PV/T was not yet a mature technology. The trend for progress in PV/T is currently strictly constrained because of various inherent practical difficulties. Additionally, temperature maldistribution and rise between the inlet and outlet still exist in the fluid-based arrangements. Thus, the decline in PV cell efficiency is mainly caused by a difference in coolant temperature over time [4]. Furthermore, high coolant temperature operation results in a low heat dissipation effectiveness, which causes a low thermal efficiency [16]. Additionally, the insecurity and irregular nature of territorial conditions continue to limit the deployment of PV/T systems. Furthermore, current electric and thermal energy storage technologies are insufficient to meet market demand [16]. Therefore, more extensive research is needed to fill the research gap in PV/T by manipulating key factors such as terrestrial parameters (ambient temperature, wind speed, and many others). Hassani et al. [17] evaluated a PV/T's life cycle exergy using three system configurations. The authors presented a new second thermal component. They explored water and Ag/water nanofluids as optical filters in their new thermal unit. They reported that the optical filter unit is a reliable and practical solution for providing a substantial amount of effective thermal energy. Ahmed and Radwan [18] modified the encapsulant materials (ethylene-vinyl acetate [EVA] and tedlar polyester tedlar [TPT]) of PV cell structure with nanocomposite to increase heat dissipation from the PV body. A satisfactory increase in the heat dissipation from the PV and electrical and thermal outputs of the PV/T was reported. Sopian et al. [19] introduced a newly discovered and enhanced PV/T with double air ducts for more effective heat dissipation. The double-pass PV/T provided a more remarkable thermal and electrical performance over the single-pass. Based on the literature, most PV/T system research focused on the performance of working fluids [20,21] and some geometry/design parameters [17–19]. Additionally, three-dimensional computational fluid dynamics (CFD) is rarely used in PV/T investigations. Besides the working media and design investigations, extensive research was conducted to control heat dissipation and losses by using a robust insulation mechanism. The rear thermal insulation is normally mounted on the backside of the PV/T collector surface to reduce backside thermal losses. Effective insulation along with robust cooling systems improves the overall conversion efficiency of PV/T systems.

When the thermal performance of the PV/T was compared with that of other absorber designs/structures, the vast majority of structural adjustments were aimed at minimizing thermal losses and thus improving the PV/T performance. Reduced thermal losses could be achieved by reducing the convection losses or by minimizing the thermal radiation losses, or both. Several innovative approaches to minimizing thermal losses have been proposed, including uncovered hybrid collectors [22], dual heat extraction [23], low-emissivity coatings [24], and variable film insulation [25]. Low-emissivity coatings were commonly used to minimize thermal radiation losses from the PV/T architecture. Alternatively, the film insulation or rear side insulation was used to reduce convection losses.

Vacuum cavity insulation (VCI) arrangements, similar to selective insulation material features, are innovative and promising insulation technology that can replace conventional low-performance insulation materials. The VCI is widely considered in the open literature for numerous applications [26]. VCI has one of the lowest thermal conductivity levels in the insulation industry [26]. The thermal conductivity in the initial condition is approximately 4 mW/(m K), whereas standard insulation supplies have a thermal conductivity of approximately 35–40 mW/(m K) [27]. The lower thermal conductivity provides more possibilities for achieving better insulation and a more useable area beneath the PV/T. The vacuum thermal insulation potential has gradually been used for windows and building walls [28]. Additionally, vacuum insulation has been considered for certain elements, such as building façades [28], glass boards [29], and smart windows for residential and commercial buildings [30]. However, an effective leak-free high vacuum insulating layer is required. Leakage across solder glass seals was reported after an attempt to use a vacuum enclosure in PV/T [31]. An innovative lead-free high-temperature sustainable fusion edge seal for vacuum insulation was reported by Memon and Eames [32].

Relying on the extensive literature in the field and to the best of the author's knowledge, the fusion edge-sealed vacuum insulation concept dose not considered for the concentrated PV thermal systems particularly. Furthermore, the current work's model combine two different model of for CPV/T systems and VCI in on arrangement so-called VCPV/T. In fact, the CPV/T and VCI were developed and analyzed separately by different researchers, but no attempt has been made to calculate the comparative performance of vacuum insulation in the CPV/T system. The comparative data between CPV/T systems and VCPV/T does not be considered yet.

Thus, the present study introduces a mathematical model for energy simulation of fusion edge-sealed vacuum insulated CPV/T (VCPV/T) system. All factors and parameters affecting a VCPV/T system's energy performance were considered. The VCPV/T is compared with the PV/T in this study in terms of economic advantages. Compared with the CPV/T system, this study presents a novel VCPV/T system based on new concepts to improve thermal and electrical performance. In this study, the fusion edge-sealed vacuum enclosure was used within the CPV/T collector to improve the overall conversion efficiency and reduce energy losses. The presence of a vacuum above the PV in a CPV/T collector can improve thermal efficiency by reducing gaseous conduction and convection between the CPV part and glass cover. Previous studies on the CPV/T system application have not considered the fusion edge-sealed vacuum enclosures. This study also presents a complete energy and exergy analysis. Additionally, the comparison of a standard CPV/T system with a new VCPV/T system is presented in this study.

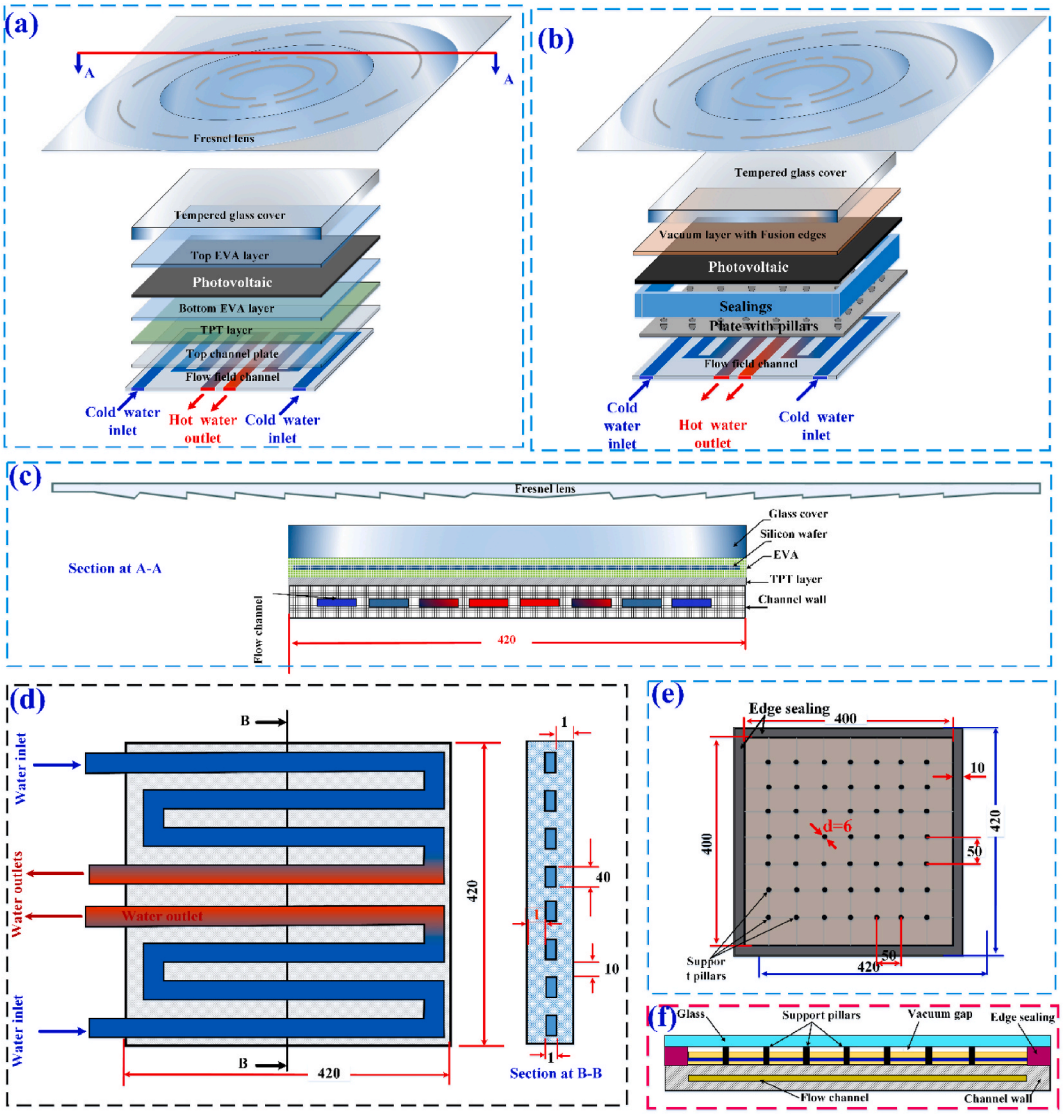

Fig. 1. Schematic of (a) the CPV/T components, (b) the fusion vacuum edge-sealed layer VCPV/T components, (c) side view of the CPV/T indicating the layers and flow channels, (d) coolant flow channel, and (e) the pillar location in the vacuum space.

Table 2
Thermal properties and dimensions for CPV/T and VCPV/T.

Layers	Detailed dimensions (mm)		Properties		
	CPV/T module	VCPV/T module	ρ (kg/m^3)	C_p (J/kg. K)	k (W/m k)
Tempered glass cover	3	3	3000	500	2
Vacuum layer	–	0.3	–	–	Eq. (9)
Top EVA	0.5	0.5	960	2090	0.311
Silicon wafer	0.2	0.2	2330	677	130
Bottom EVA	0.5	0.2	960	2090	0.311
Tedlar	0.3	–	1200	1250	0.15
Aluminum channel	1	1	2179	871	202.4
Fluid layer	1	1	Ref. [30]	Ref. [30]	Ref. [30]

2. Physical model

Fig. 1 shows the conventional CPV/T and the newly proposed VCPV/T systems in this study. The conventional CPV/T system consists of a glass layer, top and bottom EVA layers, a silicon wafer, a Fresnel lens as a concentrator, and a TPT layer with thicknesses

Table 3
Parameters and material properties of the components used in the CFD model for vacuum insulation layer [32].

Parameter	Description	Value/Type
Glass sheet	Thermal conductivity	1 W/m k
Emittance	Two surfaces (Hard coating)	0.15/SnO_2
Fusion edge seal	Material	Sn90–In10 wt% alloy
	Width	10 mm
	Thermal conductivity	62.8 W/m k
	Thermal Transmittance	1.039 W/m^2 k
Fusion seal composition	$B_2O_3$38–Sn62 wt% mixture	
Support Pillar	Material	Stainless steel 304
	Diameter	0.3 mm
	Height	0.15 mm
	Pillar separation	24 mm
	Thermal conductivity	16.2 W/m k

Table 4
PV layer reflectivity (R), absorptivity (α), transmissivity (τ), and emissivity (ε) as detailed presented in Ref. [37].

Layer	(R)	(α)	(τ)	(ε)
Glass	0.04	0.04	0.92	0.85
EVA	0.02	0.08	0.90	
Silicon	0.08	0.90	0.02	
TPT	0.86	0.128	0.012	0.9
Aluminum	–	–	–	0.9

and thermal properties presented in Table 1 and Table 2. The PV module has a thermal absorber attached to it, which is used to control the temperature of the module using pure water as a cooling fluid. The top and bottom EVA layers surrounding the silicon wafer, which generates electricity, respectively protect and provide electrical insulation [33]. The EVA and TPT layers have low thermal conductivities (Table 2), which explains why less heat is transferred to the flowing water in the thermal absorber system. Thus, this results in a higher PV cell temperature, lowering the obtained electric power and cell's lifetime. Furthermore, energy loss to the surrounding air through the glass reduces the system's efficiency.

In the proposed VCPV/T system, the conventional CPV/T system is modified by adding a vacuum layer and changing the thickness of the EVA layer (Fig. 1). The vacuum layer is between the top EVA layer and the glass, which helps in minimizing the amount of heat loss to the surrounding air. However, this modification may increase the silicon wafer temperature, decreasing the produced electricity. To avoid this risk, the thickness of the bottom EVA layer is reduced and the TPT layer is removed. This lowers the thermal resistance underneath the silicon wafer, allowing more heat to be transferred to the thermal absorber and keeping the PV module temperature under safe limits. Table 2 provides the dimensions and thermal properties of the newly proposed VCPV/T system.

An important criterion in developing the VCPV/T system is vacuum sealing. This is due to the thermally generated external tensile and compressive strains that previous vacuum sealing materials, such as Cerasolzer and Solder Glass, endured. In this study, a new high-temperature-based fusion edge-sealed vacuum insulation is proposed. The fusion edge-sealed vacuum glazing was constructed using bonded Sn62–$B_2O_3$38 wt% textured surface fused with Sn90–In10 wt% alloy at 450 °C with a hot-plate surface heat induction of 50 °C ± 5 °C and a cavity vacuum pressure of $8.2{\cdot}10^{-4}$ Pa [31]. An array of stainless steel support pillars with a height of 0.15 mm and a diameter of 0.3 mm was placed 50 mm apart [34,35]. Table 3 shows the parameters of the fusion edge-sealed vacuum insulation layer. The active area of the PV module in both systems is approximately 435 × 435 mm^2. The thermal absorber for both systems used in this study consists of two serpentine flow fields with a channel height and width of 1 and 50 mm, respectively. The thermal absorber comprises two aluminum channels with a 1 mm wall thickness and a 5 mm separation between each flow channel.

3. Theoretical analysis

In this study, both conventional CPV/T and VCPV/T systems were modeled and comprehensively investigated. The reflected, absorbed, and transmitted solar radiation through the different layers of both systems are based on the optical properties of each layer, which are provided in Table 4. Based on the system layers' optical properties, the incident solar radiation is transmitted from the glass layer to the top EVA layer, and then most of the received radiation is transmitted to the silicon wafer. The silicon wafer absorbs most of the transmitted solar radiation from the top EVA layer, converting part of it into electricity and the rest into heat. This heat increases the cell temperature, which degrades the electrical efficiency and necessitates an efficient method to regulate the cell temperature under safe conditions.

During the simulation, conduction, convection, and radiation heat transfer were considered under the following assumptions:

1. The properties of the solid parts are temperature independent.
2. The conventional CPV/T and VCPV/T systems' backside is sufficiently insulated to ensure that all of the heat is transferred to the water in the thermal absorber.

3. The water flow in the thermal absorber is assumed to be laminar and incompressible, with a Reynolds number of (*Re*) 75 in both serpentines.
4. Water thermal properties are assumed to be temperature-dependent following the same polynomial equations mentioned in Ref. [36].

3.1. Governing equations

The governing equations for both CPV/T and VCPV/T layers, the fluid flow, and solar cell thermal performance equations are presented.

3.1.1. Solid layers

Heat is transferred through solid layers, including the edge sealing and aluminum pillars, via conduction, and unsteady three-dimensional energy [Eq. (1)] is presented [35].

$$\nabla.\left(k_i\,\nabla T_i\right)+q_i=0 \tag{1}$$

where k_i, T_i, and q_i are the thermal conductivity, temperature, and heat generation in each layer, respectively. The amount of solar radiation absorbed by the layer represents the heat generated in each layer. The values of heat generation in each layer are calculated from Eqs. (2)–(4).

$$\text{Glass layer}: q_g=\frac{G\times\alpha_g\times A_g}{V_g} \tag{2}$$

$$\text{Top EVA layer}: q_{top\_EVA}=\frac{G\times\alpha_{EVA}\times\tau_g\times A_{EVA}}{V_{EVA}} \tag{3}$$

$$\textit{Silicon layer}: q_{sc}=\frac{(1-\eta_{sc})\times G\times\alpha_{sc}\times\tau_{EVA}\times\tau_g\times A_{sc}}{V_{sc}} \tag{4}$$

where A and V denote the surface area and volume of each layer, respectively, and G denotes the solar radiation incident on the glass surface. The cell efficiency is the ratio of output electrical energy to total solar energy received, which can be calculated based on the cell temperature from Eq. (5) [36].

$$\eta_{sc}=\eta_{ref}\left(1-\beta_{ref}\left(T_{sc}-T_{ref}\right)\right) \tag{5}$$

where η_{ref} and β_{ref} denote the PV efficiency and cell temperature coefficient, respectively, at a reference temperature, T_{ref} of 25 °C. Because the values of η_{sc}, q_{sc}, and T_{sc} are related to each other, their estimation is based on an iterative technique described in Ref. [18].

3.1.2. Fluid domain

The flow of water in the thermal absorber containing two serpentines is governed by Eqs. (6)–(8):

Continuity equation:

$$\nabla.\left(\rho\vec{V}\right)=0 \tag{6}$$

Fluid momentum equations

$$\vec{V}.\nabla\left(\rho\vec{V}\right)=-\nabla P+\nabla.\left(\mu\nabla\vec{V}\right) \tag{7}$$

Fluid energy equation

$$\vec{V}.\nabla\left(\rho C_f T_f\right)=\nabla.\left(k_f\nabla T_f\right) \tag{8}$$

where the subscript *f* denotes the fluid domain and P, C, T, *V*, μ, and ρ denote the coolant pressure, specific heat, temperature, velocity, dynamic viscosity, and density, respectively.

3.1.3. Vacuum layer

Heat is transferred via radiation between the glass layer's bottom surface and the EVA layer's top surface. A surface-to-surface (S2S) model, which considers the emissivity effect and view factor, is used to model the radiation process in any gap [38,39]. The emissivity of the inner glass surface is assumed to be 0.18, and the thermal conductivity of the vacuum layer is calculated from Eq. (9).

$$k_{vacuum}=\frac{k_o}{1+\frac{\left(1.07\times10^{-7}\right)\times T}{l_{vacuum}\times P}} \tag{9}$$

where T is the absolute average temperature between the glass layer and EVA top layer, l_{vacuum} is the vacuum gap thickness (height of 0.15 mm and diameter of 0.3 mm) implemented to be 0.0003 m, and P is the vacuum pressure implemented in the model to be 0.00082

Pa; a detailed description of the achievable vacuum pressure is published by Memon and Eames (2020) [32]. k_o is the reference air thermal conductivity, which is 0.026 W/m k. Details of the S2S model can be found in Ref. [40].

3.2. PV module characterization

Different parameters are used to compare the conventional CPV/T and the new VCPV/T model under certain operating conditions. The electrical power, P_{el}, is calculated using Eq. (10) [41].

$$P_{el} = \eta_{cell} \cdot G \cdot \alpha_{sc} \cdot \tau_{top} . A_{sc} \tag{10}$$

where η_{cell} is the cell efficiency calculated from Eq. (5). G, α_{sc}, and τ_{top} denote the received solar radiation to the module, cell absorptivity, and PV module packing factor, respectively. A_{sc} denotes the solar radiation receiving area.

The pumping power consumed by pumping the cooling water through the two serpentines to overcome friction is estimated from Eq. (11).

$$P_{pumping} = \left(\frac{\dot{m}}{\rho_w}\right) \times \Delta P \tag{11}$$

where $\dot{m}$ and ΔP denote the water mass flow rate and pressure drop through the thermal absorber, respectively. The simulation is obtained at the Re of 75 calculated from Eq. (12).

$$Re = \frac{\rho\, V_{in}\, D_h}{\mu} and\ D_h = \frac{4\,(W_{ch} \times H_{ch})}{2(W_{ch} + H_{ch})} \tag{12}$$

where $V_{in}, D_h,\ W_{ch},$ and H_{ch} denote the water velocity inlet, hydraulic diameter, channel width, and height, respectively. The gained power from the entire PV system is calculated using Eq. (13).

$$P_{net} = P_{el} - P_{pumping} \tag{13}$$

The thermal heat gained by the cooling water through the thermal absorber is estimated from Eq. (14).

$$P_{th} = \dot{m} \cdot C_{p,w} \cdot (T_{out} - T_{in}) \tag{14}$$

The heat loss from the top glass layer is obtained by combining both convection and radiation heat transfers and calculated using Eq. (15).

$$Q_{th,loss} = h_w . A_g . (T_g - T_a) + \varepsilon_g . \sigma . A_g . \left(T_g^4 - T_s^4\right) \tag{15}$$

where h_w, A_g, T_g, T_a, ε_g, and T_s are the convection heat transfer coefficient, glass area, glass temperature, ambient temperature, the emissivity of the external glass layer, and sky temperature, respectively.

The convection heat transfer coefficient to the surrounding air, h_w, is obtained as a function of the wind speed, U_w, and it increases with an increase in wind speed, which influences the PV system's performance and can be calculated using Eq. (16) [37,42].

$$h_w = 5.7 + 3.8 \times U_w \tag{16}$$

3.3. Exergy analysis

Exergy assessment is frequently conducted to control the losses within any energy system using a complete energy figure. The electrical exergy (Ex_{el}) is normally considered as a pure exergya nd s equivalent to P_{el} [2,3]. Furthermore, the thermal exergy (Ex_{th}) is defined by Eq. (17) which is general description used for Ex_{th} [3].

$$Ex_{th} = Ex_{ma,ex} - Ex_{ma,\ in} = \dot{m}_f (\Psi_{out} - \Psi_{in}) \tag{17}$$

The Ψ_{out} *and* Ψ_{out} are the flow exergy terms which are be defined as:

$$\Psi_{out} = (h_{out} - h_{amb}) - T_{amb}(s_{out} - s_{amb}) \tag{18}$$

$$\Psi_{in} = (h_{in} - h_{amb}) - T_{amb}(s_{in} - s_{amb}) \tag{19}$$

The WF mean temperate (T_m) can be calculated by the following equation:

$$T_m = \frac{h_{out} - h_{in}}{S_{out} - S_{in}} = \frac{(T_{f,out} - T_{f,in})}{\ln\left[\frac{T_{f,out}}{T_{f,in}}\right]} \tag{20}$$

$(h_{out} - h_{in})$ and $(S_{out} - S_{in})$ describe to the enthalpy and entropy differences over the WF from, respectively. By rewriting eq (17) from eqs (18) and (19), it is found that E_{xth} is equal to the P_{th} multiplied by the Carnot factor. Ex_{th} can be attained as [43].

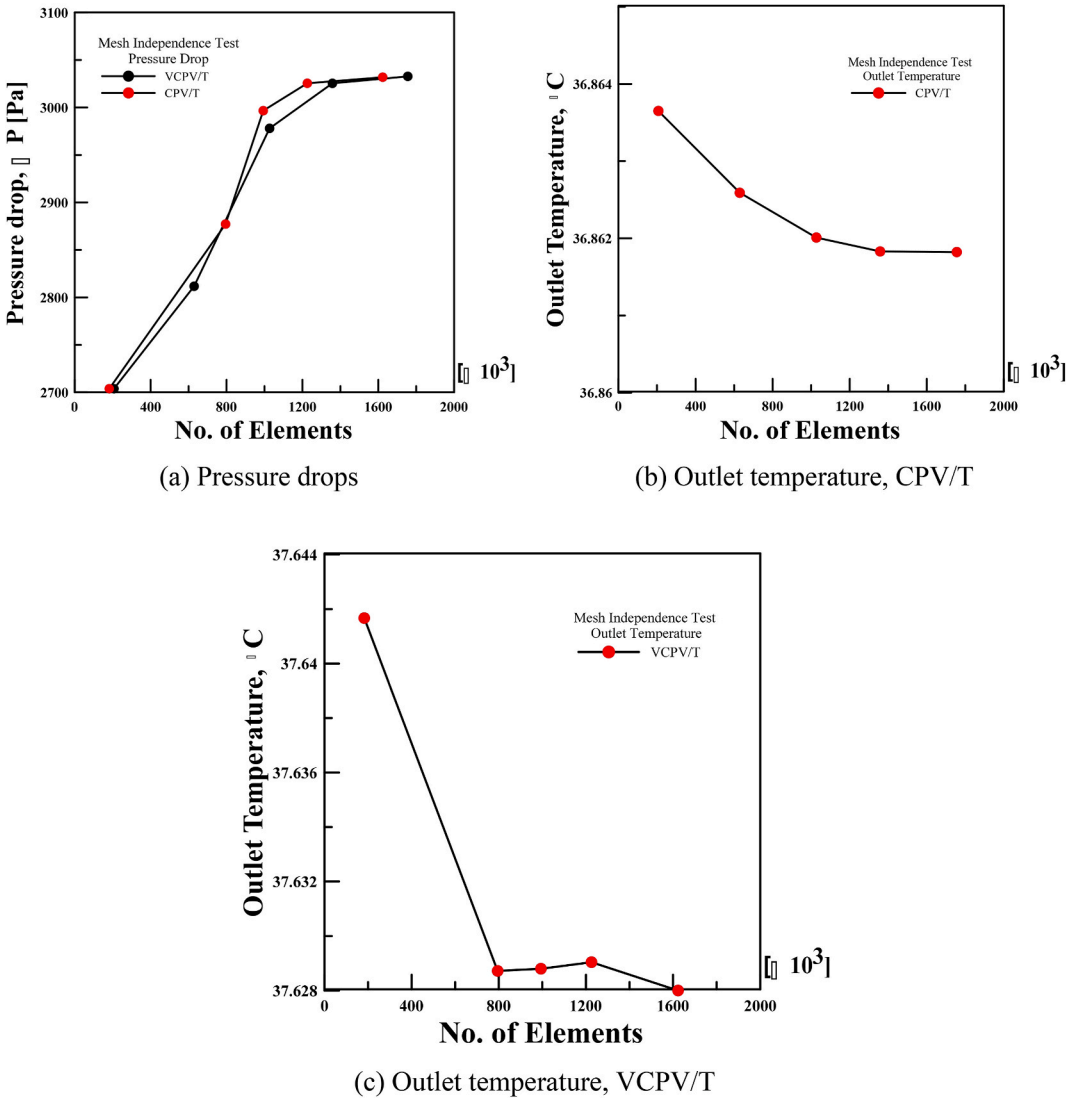

Fig. 2. Mesh independence test at CR 1 showing (a) pressure drop versus number elements comparing CPV/T with VCPV/T, (b) outlet temperature versus some elements test with CPV/T, and (c) outlet temperature versus some elements test with VCPV/T.

$$Ex_{th} = \underbrace{\dot{m_f} \cdot C_f \cdot \left(T_{f,out} - T_{f,in}\right)}_{thermal\ power} \cdot \underbrace{\left(1 - \frac{T_0}{T_m}\right)}_{carnot\ factor} \tag{21}$$

where $T_{f,in}$, $T_{f,out}$, and T_m denote the coolant inlet, outlet, and mean temperature, respectively. The solar radiation cannot be expressed as pure exergy [4,5]. Thus, the coefficient of radiation exergy (Ψ_s) must be involved in calculating the exergy content received from the sun. Ψ_s is implemented as shown in Eq. (18) [4].

$$\psi_s = 1 - \frac{T_a}{T_{sun}} \tag{22}$$

The solar radiation temperature (T_{sun}) is 6000 K; subsequently, the value of Ψ_s is 0.95 [44].

3.4. Cost analysis

The payback period (PP) for the installation of the PV/T and VPV/T systems can be used to determine the life cycle of a system. It can be calculated using the following equation [45]:

$$payback\ period\ (PP) = \frac{\ln[(CF)/(CF - P \times i)]}{\ln(1+i)} \tag{23}$$

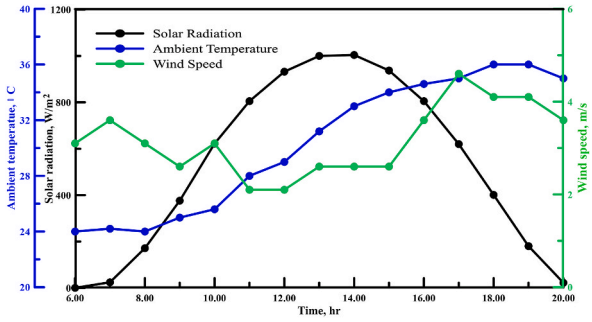

Fig. 3. Illustration of the hourly variation of solar radiation, ambient temperature, and wind speed obtained on July 10, 2019 in Cairo, Egypt, where the tests were conducted for CPV/T and VCPV/T.

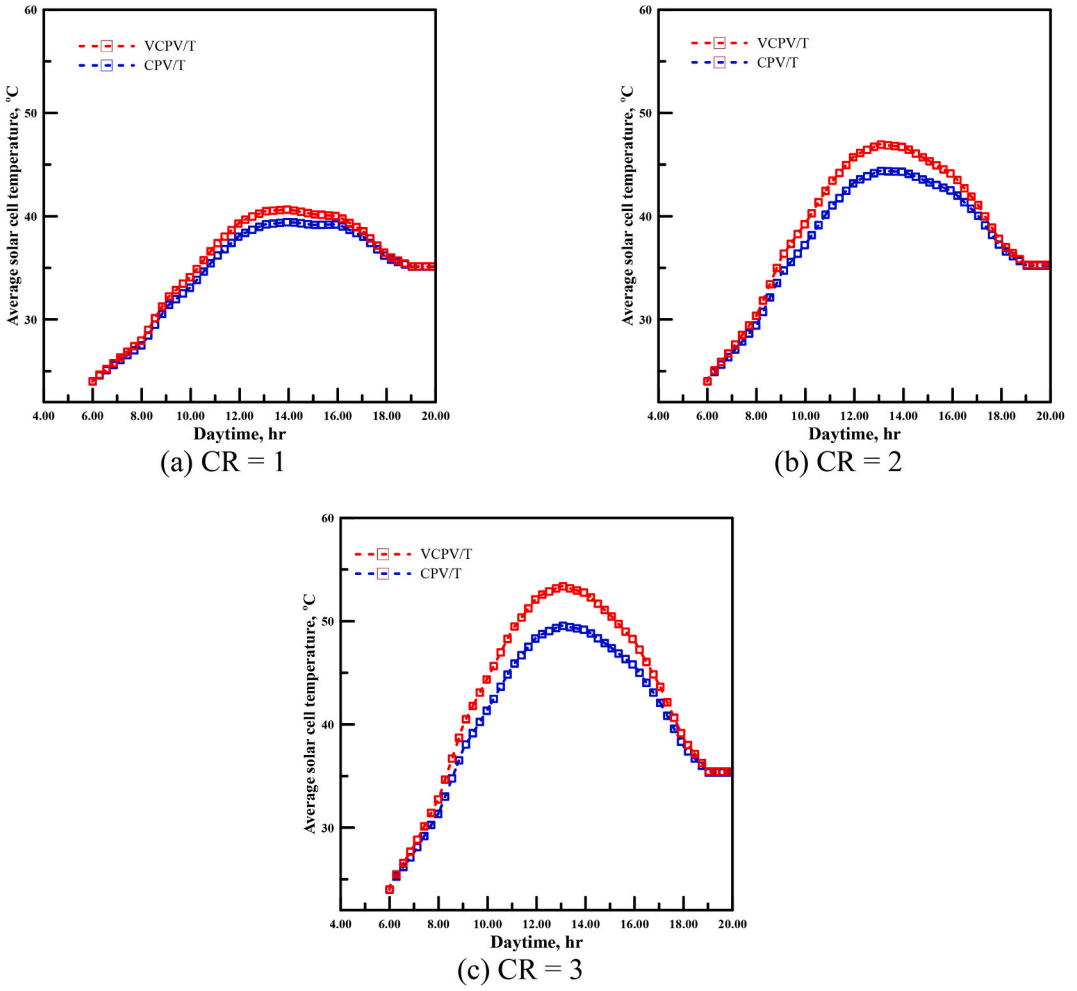

Fig. 4. *Influence of average solar cell temperature on VCPV/T compared with CPV/T system at (a) CR = 1, (b) CR = 2, and (c) CR = 3.*

where P is the initial cost for both the conventional and the modified systems, i is the annual rate of interest, and CF is the annual cash flow that is determine by

$$CF = R - M \tag{24}$$

where R and M are the annual revenue based on adding vacuum glazing to the PV/T system and the annual operating cost, respectively.

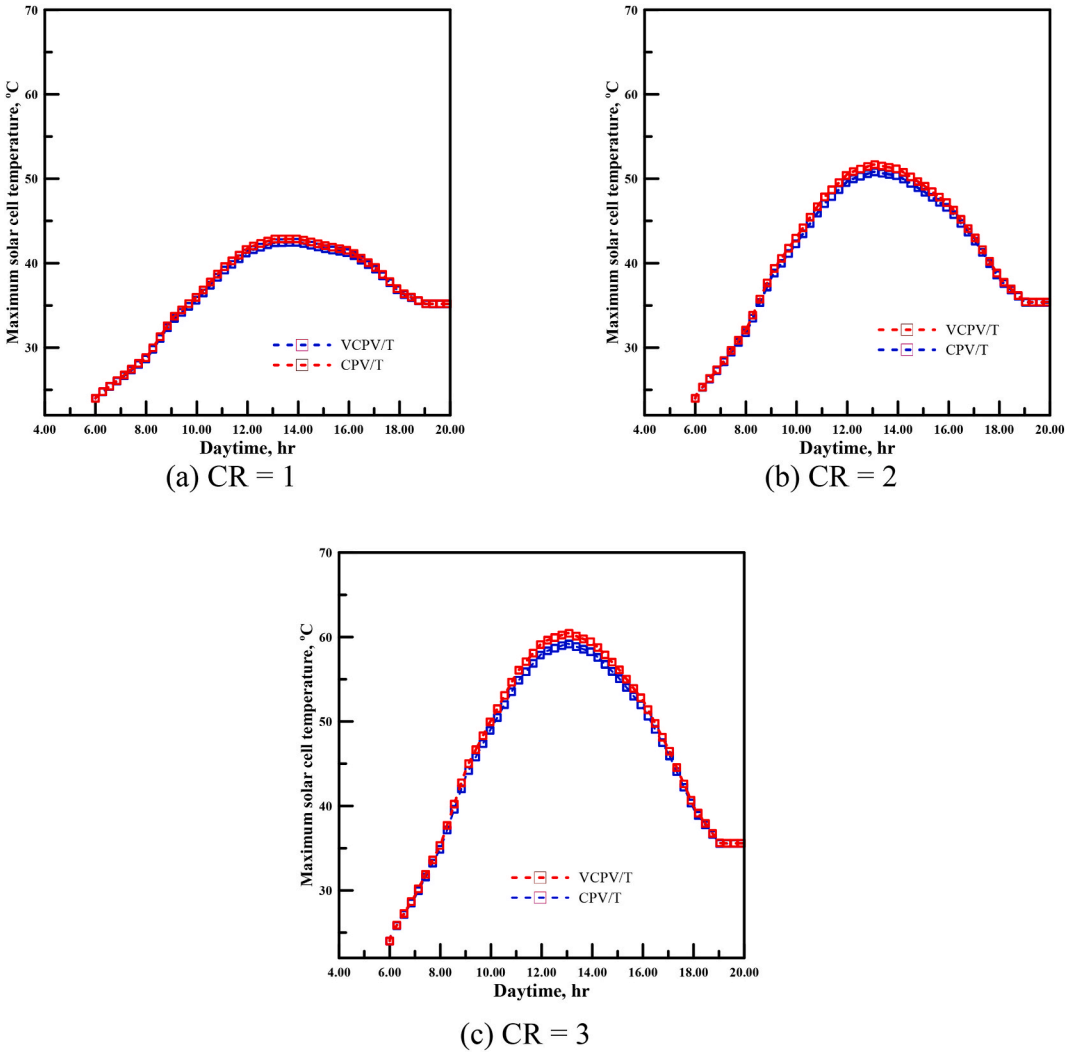

Fig. 5. *Transient variation of maximum cell temperature on VCPV/T compared with CPV/T at (a) CR = 1, (b) CR = 2, and (c) CR = 3.*

3.5. Boundary conditions

Both CPV/T and VCPV/T systems are subjected to transient boundary conditions. Water at uniform velocity and constant temperature of 30 °C is projected at the inlet of the thermal absorbers for both serpentines. The outlet of both serpentines is defined as zero-gauge pressure. The heat generation in each layer of the PV/T and VCPV/T systems is estimated at selected concentration ratios (CRs) of 1, 2, and 3. The top glass layer is used to account for heat losses by convection and radiation. Temperatures and heat fluxes are shared between every consequent layer via thermally coupled boundary conditions. The heat absorber's backside and the PV's side are predicted to be adiabatic. The solar radiation, wind speed, and ambient temperature change with time during the day, and they are taken on the 10th of July in Cairo, Egypt (30.0444 °N, 31.2357 °E).

3.6. Validations and grid independent study

The current model results were verified with the data of experimental work that were conducted by the author [46]. Furthermore, the current model simulation results were compared with experiments and numerical of [47] and of [48], respectively. The validations showed a maximum relative deviation between the authors experimental work and literature work and the current study is less than 3.5%. The validations are discussed in detail in previous author work [49,50].

A grid independent study is conducted for both CPV/T and VCPV/T at $Re = 75$ to determine the appropriate mesh size for modeling and simulation analyses. The numerical results show the number of mesh to be selected for this study. Fig. 2 shows that increasing the number of elements above 1.36 and 1.23 million for both conventional CPV/T and VCPV/T systems, respectively, has a minor effect on the obtained thermal power and pressure drop. Therefore, the number of elements chosen is sufficient to accurately simulate conventional CPV/T and VCPV/T systems.

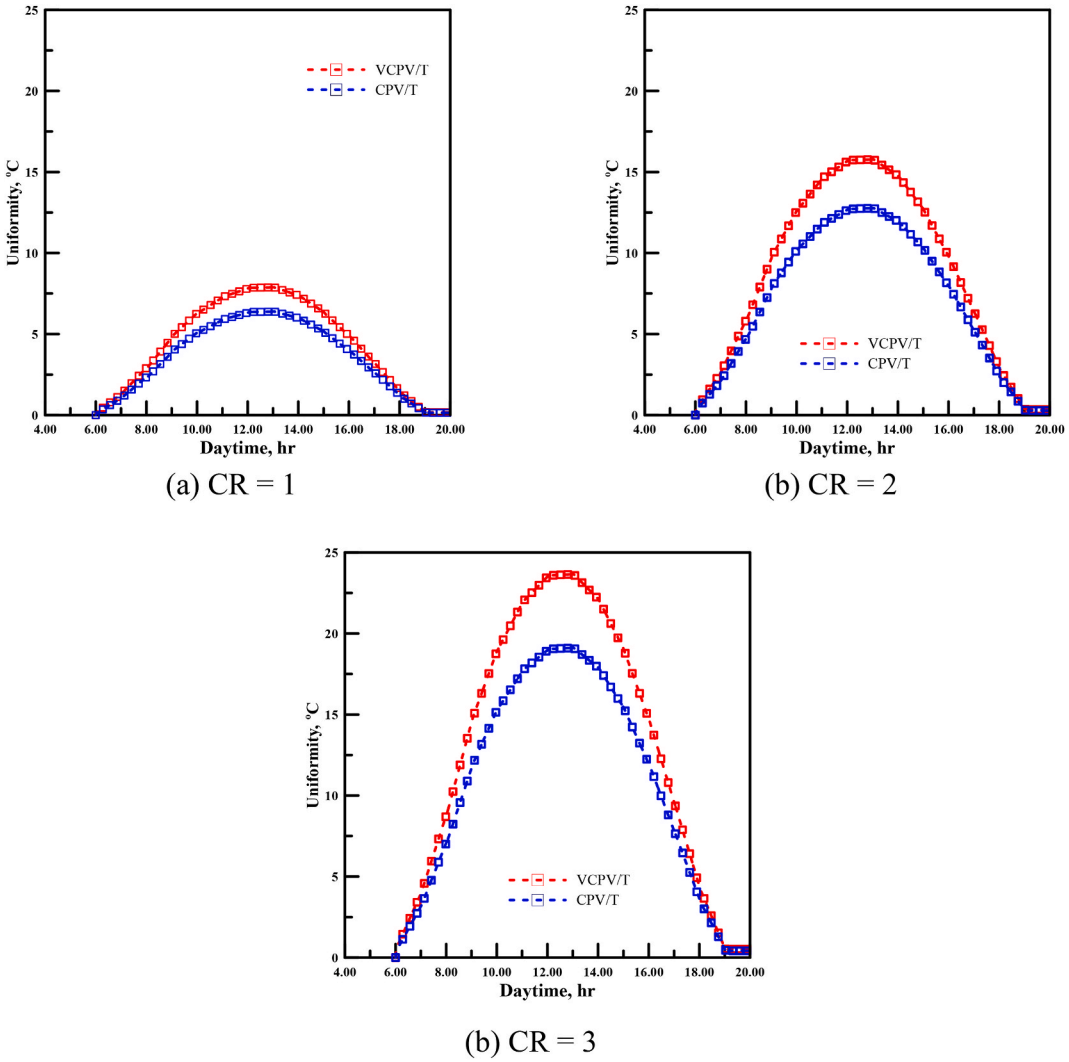

Fig. 6. Hourly variation of uniformity over the solar cell on VCPV/T and CPV/T at (a) CR = 1, (b) CR = 2, and (c) CR = 3.

4. Results and discussion

This section compares the proposed VCPV/T system with the conventional CPV/T system in terms of transient instantaneous simulation. The average solar cell temperature, minimum and maximum cell temperature, glass temperature, cooling water outlet temperature, uniformity on the cell, heat loss, and heat gain are calculated at different CR ratios (1, 2, and 3) and a constant *Re* of 75. Fig. 3 plots the hourly variation of solar radiation, ambient temperature, and wind speed obtained on the 10th of July in Cairo, Egypt. These hourly values are imported into the ANSYS FLUENT to update the boundary conditions hourly.

4.1. The influence of average solar cell temperatures on VCPV/T compared with CPV/T

Fig. 4 shows the hourly variation of average solar cell temperature at different CR values at *Re* of 75. The figure shows that the average solar cell temperature was higher with VCPV/T than with CPV/T at all CR values because of the lower heat loss characteristics of the vacuum layer. However, incoming solar irradiation is higher with CPV/T than with VCPV/T. This is due to a reduction in heat loss via the glass and a direct transfer of the heat to the solar cell. As the solar irradiance increases, the difference in average cell temperature between the CPV/T and VCPV/T systems increases with time until it reaches its maximum value at around 14:00 h, after which it reduces. This difference increases with an increase in the CR ratio, reaching 2.53%, 5.88%, and 7.86% for CRs of 1, 2, and 3, respectively.

4.2. Effects of transient variation of maximum solar cell temperatures on VCPV/T in comparison with CPV/T at CRs of 1, 2, and 3

Fig. 5 shows the transient variation of the maximum solar cell temperature for various CR values. At low CR (CR = 1), both CPV/T and VCPV/T exhibit nearly identical systems performance in terms of maximum solar cell temperatures, and the difference between

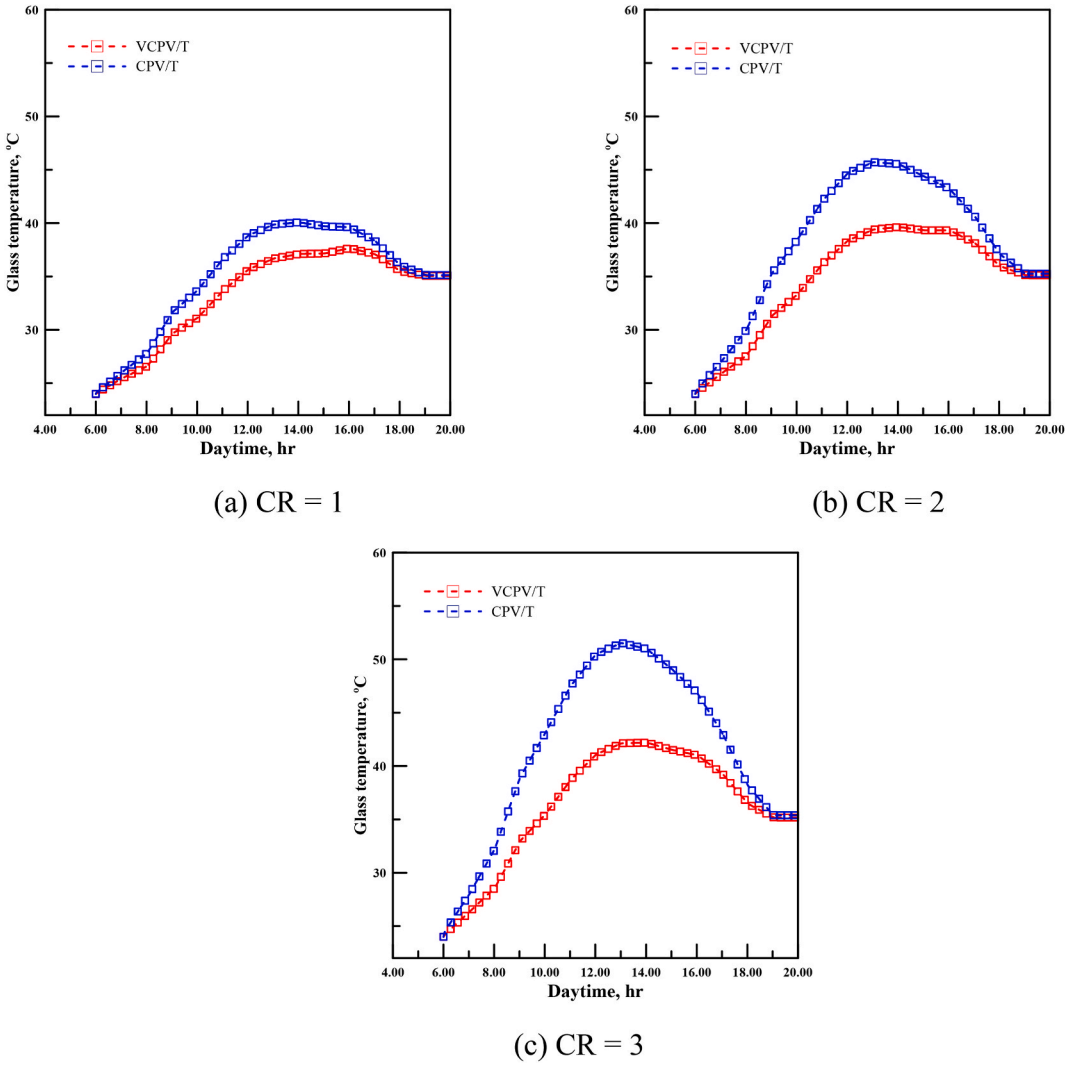

Fig. 7. The influence of top glass surface temperatures on the solar cell in the VCPV/T and CPV/T showing hourly variations at (a) CR = 1, (b) CR = 2, and (c) CR = 3.

both systems increases with an increase in CR. VCPV/T system provides higher values of maximum solar cell temperatures compared with the CPV/T system, and this is because the effect of the vacuum layer minimizes heat loss through the glass and increases heat toward the solar cell. The percentage increase in maximum cell temperature between the two systems is 1.0%, 1.7%, and 2.16% at CRs of 1, 2, and 3, respectively.

4.3. Effects of uniformity of solar cell temperatures on VCPV/T compared with CPV/T at CRs of 1, 2, and 3

The uniformity of solar cell temperature, which is represented by the difference between the maximum and minimum cell temperatures, is considered an important factor in determining the occurrence of thermal stresses on the solar cell. Fig. 6 shows the plots of the hourly variation of temperature uniformity over the day. The figure shows that uniformity increases with time until it reaches a maximum value and then decreases. The value of uniformity increases with an increase in CR.

4.4. Effects of top glass surface temperatures on VCPV/T compared with CPV/T at CRs of 1, 2, and 3

The top glass surface temperature is lower with the new VCPV/T system than with the CPV/T system. This is due to the vacuum layer used between the glass and top EVA layers. Fig. 7 presents the transient behavior of the top glass layer for all tested CR values. The results show that an increase in CR values increases the glass temperature, and the difference between VCPV/T and CPV/T glass temperatures also increases with the CR value, as presented in Fig. 7.

4.5. Thermal heat loss and heat gain analysis on VCPV/T and CPV/T at CRs of 1, 2, and 3

Figs. 8 and 9 show the transient hourly thermal heat loss and gain from the top surface of VCPV/T and CPV/T, respectively. Fig. 8 shows that the proposed VCPV/T system achieved lower heat loss through the glass layer than the CPV/T system. This is due to the

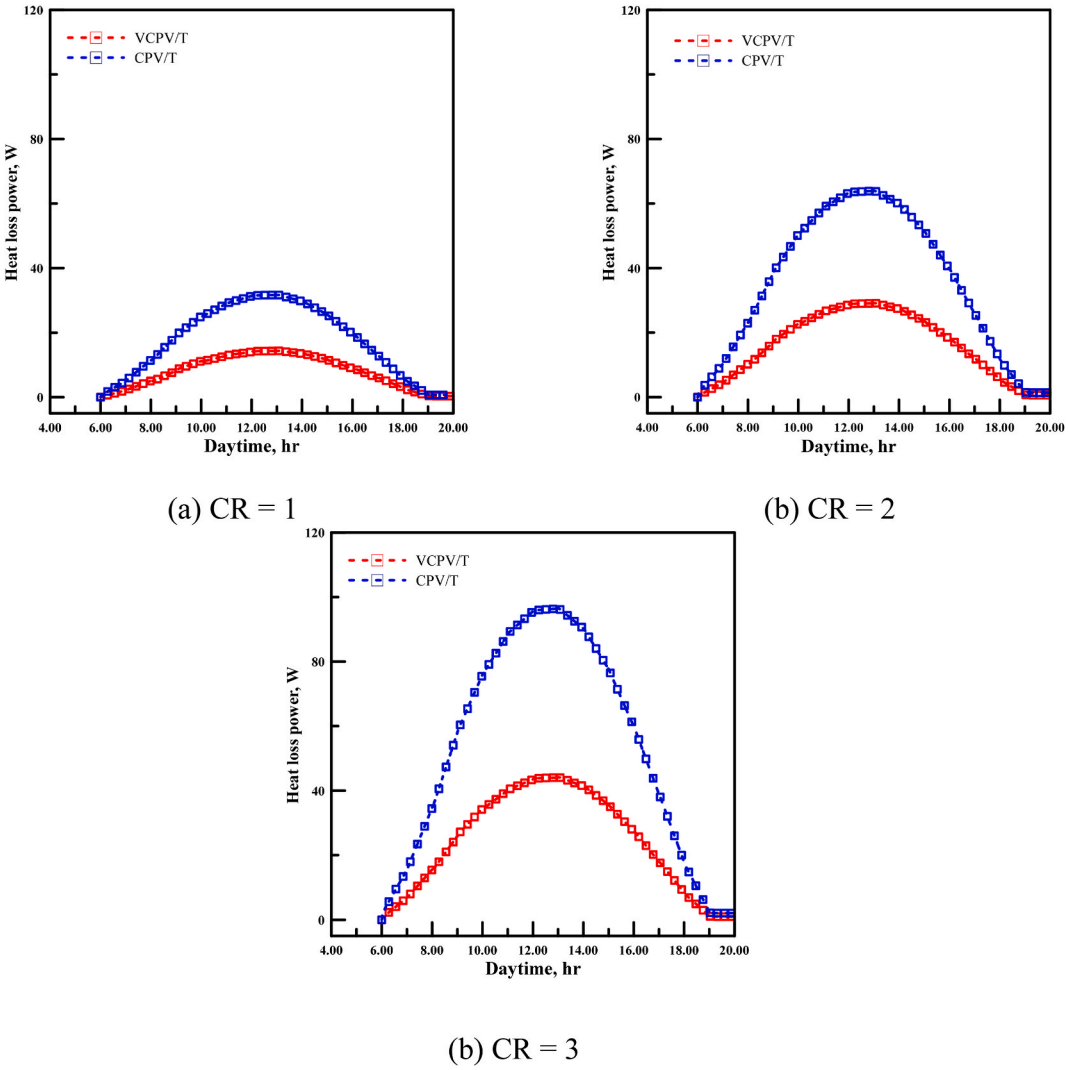

Fig. 8. Transient variation of thermal heat loss power at (a) CR = 1, (b) CR = 2, and (c) CR = 3 for VCPV/T and CPV/T systems.

effect of adding a vacuum layer between the solar cell and the glass, which acts as an insulator and prevents heat from passing through the glass layer. This effect can be seen in the heat dissipated to the cooling water, which is higher with the VCPV/T system than with the CPV/T system (Fig. 9).

4.6. Electrical and thermal exergy analysis of VCPV/T and CPV/T

Fig. 10 shows that variations in the received radiation effect significantly impact the thermal, electrical, and overall exergies of the two studied systems. Fig. 10(a) shows the results at CR = 1,2, and 3 where the diffence of electrical exergy between the VCPV/T and CPV/T is very insignificant. However, there is a reduction in the electrical in the case of VCPV/T, but the maximum reduction is less than 2% which typically observed between 11:00 to 13; 00 time in all the studied cases. In fact, this highlights that even the vacuum insulation leads to an increase in the PV temperature, but this has very minor impact in the electrical output.

Whereas thermal exergy is predicted to be higher in VCPV/T than in CPV/T. The maximum exergy occurred at CR 1 of 70 W when higher solar heat gains were recorded at 13:00. Fig. 10 (b) shows the results at CR 2, in which the VCPV/T gained thermal exergy at a maximum of 120 W, whereas CPV/T gained at 110 W. Fig. 10 (a), (b), and (c) reveal that at CR 3, with the maximum thermal, electrical, and total exergy of 144.5, 33, and 177.6 W all around 13:00 h for the new VCPV/Thermal systems. Thermal and total exergy are both increased by approximately 14% and 10.7%, respectively, at CR = 3. However, an average reduction of approximately 1.33% occurred in the electrical exergy under the same conditions.

Finally, an economic analysis, based on the actual cost in Egypt, has be performed to evaluate the lifetime cycle of the conventional CPV/T system and the new vacuum system VCPV/T. The analysis has shown that adding vacuum glazing layer to the conventional CPV/T system increases the payback period of the system. It is estimated that the payback period increases by 1.05 years when vacuum

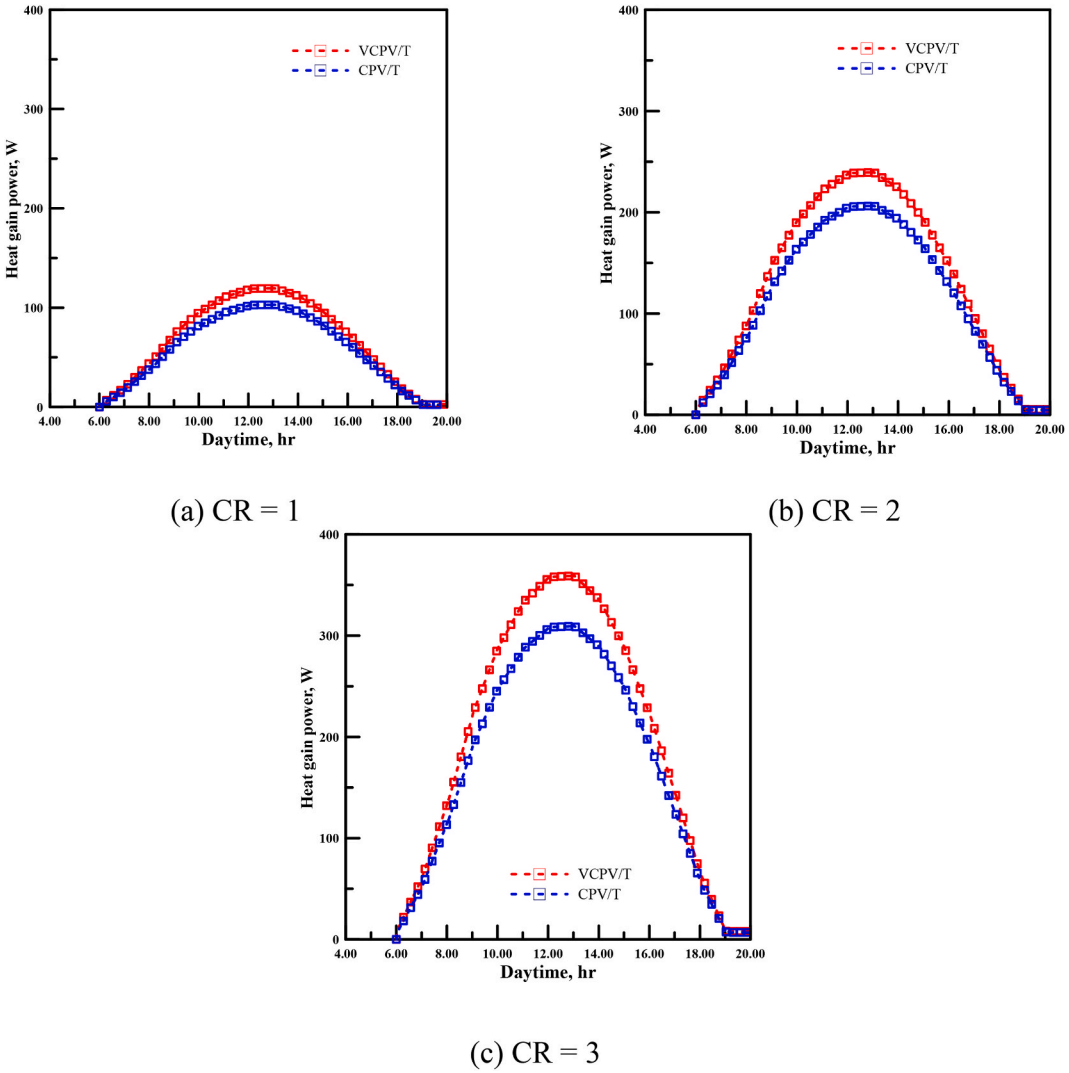

Fig. 9. Transient variation of thermal heat gain power at (a) CR = 1, (b) CR = 2, and (c) CR = 3 for VCPV/T and CPV/T systems.

glazed is used compared to the conventional CPV/T system. This period is decreased to 0.76 years when the benefits from the thermal heat gain are considered.

5. Conclusion

In this study, the hybridization potential of integrating a progressive fusion edge-sealed vacuum insulation layer to a concentrated photovoltaic solar thermal collector (VCPV/T) in contrast to a CPV/T system is investigated to achieve net-zero carbon emissions by 2050. The proposed VCPV/T system results indicate a significant reduction in heat loss via the glass layer compared with the conventional CPV/T system. The vacuum insulation layer in the CPV/T module served as an insulator, preventing heat transfer through the glass layer. This can be seen in the heat dissipated to the cooling water, which is higher with a VCPV/T system than with the conventional CPV/T system. Increasing the CR value increases the glass temperature and the glass temperature difference between VCPV/T and CPV/T. The percentage rise in maximum cell temperature between both systems is 1.0%, 1.7%, and 2.16% at CRs of 1, 2, and 3, respectively, for VCPV/T. Even though the VCPV/T shows a noticeable improvement in overall performance compared with conventional CPV/T, the vacuum enclosure increased the PV module's average temperature. This initiates a reduction in the electrical performance of the VCPV/T. For instance, at CR = 3, the maximum thermal, electrical, and total exergy are 144.5, 33, and 177.6 W all around 13:00 h for the new VCPV/Thermal systems. Furthermore, at CR = 3, thermal and total exergy increased by approximately 14% and 10.7%, respectively. However, the electrical exergy was reduced by approximately 1.33% under the same conditions.

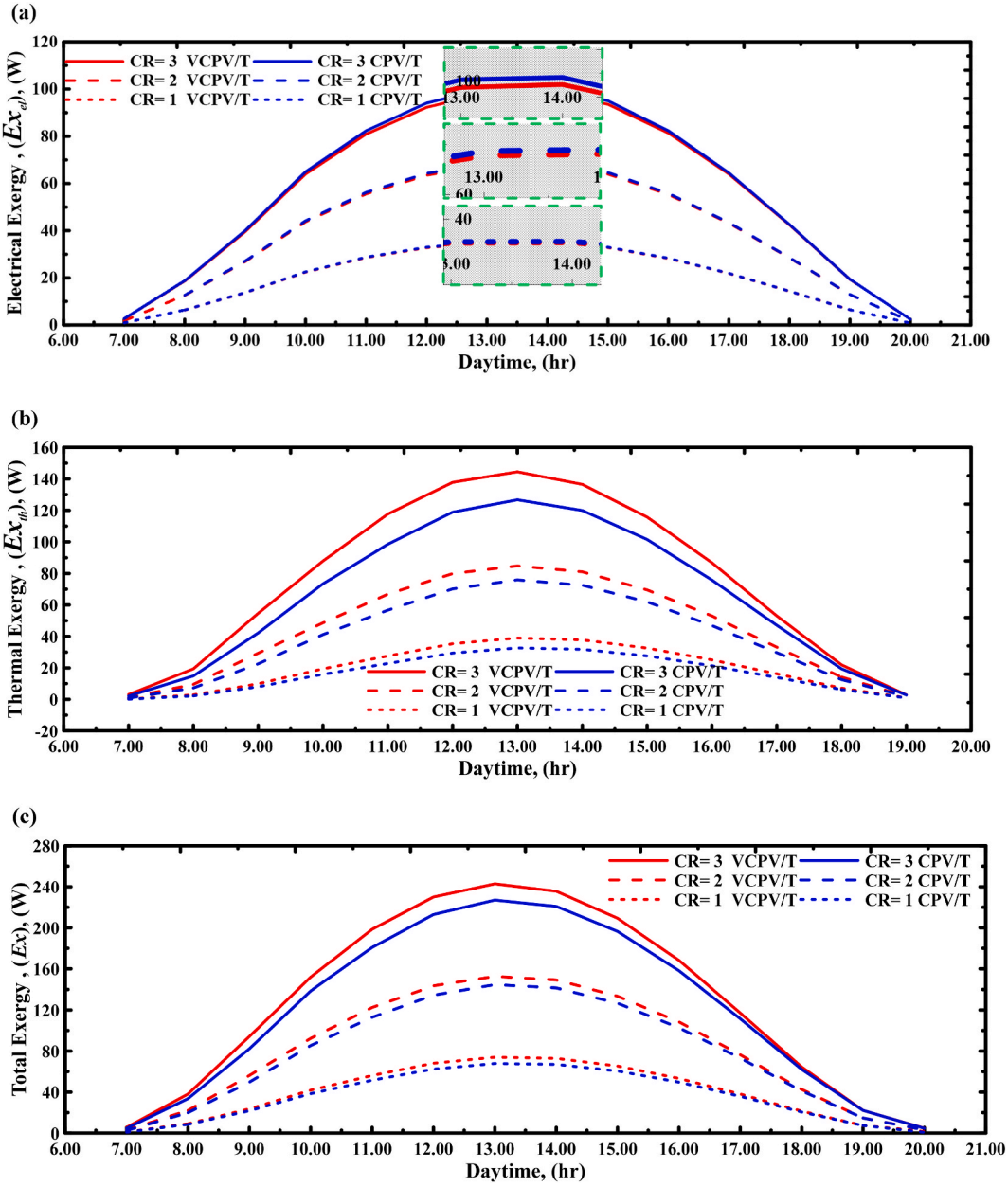

Fig. 10. *Transient variations. of (a)) Electrical exergy (b) Thermal exergy, and (a) Total exergy of VCPV/T and CPV/T under CR = 1, CR = 2, and CR = 3.*

CRediT author statement

Essam Abo-Zahhad: Methodology, Writing-Original draft preparation, Simulation, Validation, Conceptualization, Collaboration **Saim Memon**, Conceptualization, Facility, Software, and Writing-Reviewing. **Ali Radwan**: Validation, Formal Analysis, Investigation and Data Curation. **O. Abdelrehim:** Conceptualization, Funding acquisition, Investigation, Supervision, Writing-Reviewing and Editing, analysing., **Mohamed R. Elmarghany:** Conceptualization, Funding acquisition, Investigation, Supervision, Writing-Reviewing and Editing, Analysing, **Asmaa Khater:** Conceptualization, Facility, Software, and Writing-Reviewing, and **Chaouki Ghenai:** Conceptualization, Funding acquisition, Investigation, Supervision, Writing-Reviewing and Editing, analysing.

Declaration of competing interest

The authors declare that they have no known competing financial interests or personal relationships that could have appeared to influence the work reported in this paper.

Nomenclature

A	Area [m^2]
q''	heat flux transfer [Wm^{-2}]
h	convection heat transfer coefficient [$Wm^{-2}K^{-1}$]
k	thermal conductivity [$Wm^{-1}K^{-1}$]
G	solar radiation [Wm^{-2}]
P	pressure [Nm^{-2}]
R	reflectivity
S	source term in the energy equation [Wm^{-3}]
T	temperature [^{o} C]
U	thermal transmittance [$Wm^{-2}K^{-1}$]
V	volume [m^{-3}]

Greek symbols

α	absorptivity
β	cell temperature coefficient
Δ	difference
ρ	density [kg/m^3]
η	efficiency [%]
μ	viscosity [kg/m. s]
τ	transmissivity
ε	emissivity
δ	thickness [m]

Subscripts

cell	cell
g	glass
f	fluid
ref	reference
sc	solar cell
v	vacuum space

Abbreviations

CFD	computational fluid dynamics
EVA	ethylene-vinyl acetate
CPV	concentrated photovoltaic
CPV/T	concentrated photovoltaic thermal collector
CR	concentration ratio
PCM	phase change material
PV/T	photovoltaic-thermal collector
S2S	surface to surface
VCI	vacuum cavity insulation
VCPV/T	Fusion edge-sealed vacuum insulated concentrated photovoltaic-thermal collectors

References

[1] V. Kumar, N. Kaistha, Control of a concentrated solar power–biogas hybrid unit, IFAC-PapersOnLine 53 (1) (2020) 332–337.
[2] F. Karimi, et al., Experimental study of a concentrated PV/T system using linear Fresnel lens, Energy 123 (2017) 402–412.
[3] M.W. Shahzad, et al., Energy-water-environment nexus underpinning future desalination sustainability, Desalination 413 (2017) 52–64.
[4] E.M. Abo-Zahhad, et al., Thermal management of high concentrator solar cell using new designs of stepwise varying width microchannel cooling scheme, in: Applied Thermal Engineering, 2020, 115124.
[5] E. Skoplaki, J.A. Palyvos, Operating temperature of photovoltaic modules: a survey of pertinent correlations, Renew. Energy 34 (1) (2009) 23–29.
[6] M. Slaman, R. Griessen, Solar collector overheating protection, in: Solar Energy, 2009.
[7] T.T. Chow, A review on photovoltaic/thermal hybrid solar technology, Appl. Energy 87 (2010) 365–379.
[8] W. Pang, et al., A comparative analysis on performances of flat plate photovoltaic/thermal collectors in view of operating media, structural designs, and climate conditions, in: Renewable and Sustainable Energy Reviews, Elsevier Ltd., 2020, 109599.
[9] H.A. Zondag, Flat-plate PV-Thermal collectors and systems: a review, in: Renewable and Sustainable Energy Reviews, 2008.
[10] A. Kazemian, et al., Effect of glass cover and working fluid on the performance of photovoltaic thermal (PVT) system: an experimental study, in: Solar Energy, 2018.
[11] V.V. Tyagi, S.C. Kaushik, S.K. Tyagi, Advancement in solar photovoltaic/thermal (PV/T) hybrid collector technology, in: Renewable and Sustainable Energy Reviews, 2012, pp. 1383–1398.

[12] A. Kazemian, et al., in: Experimental Study of Using Both Ethylene Glycol and Phase Change Material as Coolant in Photovoltaic Thermal Systems (PVT) from Energy, Exergy and Entropy Generation Viewpoints, Energy, 2018.
[13] R. Daghigh, M.H. Ruslan, K. Sopian, Advances in liquid based photovoltaic/thermal (PV/T) collectors, in: Renewable and Sustainable Energy Reviews, 2011, pp. 4156–4170.
[14] A. Radwan, M. Ahmed, Thermal management of concentrator photovoltaic systems using microchannel heat sink with nanofluids, in: Solar Energy, Elsevier, 2018, pp. 229–246.
[15] N. Gilmore, V. Timchenko, C. Menictas, Microchannel cooling of concentrator photovoltaics: a review, in: Renewable and Sustainable Energy Reviews, 2018, pp. 1041–1059.
[16] X. Ju, et al., A review on the development of photovoltaic/concentrated solar power (PV-CSP) hybrid systems, in: Solar Energy Materials and Solar Cells, 2017, pp. 305–327.
[17] S. Hassani, et al., Environmental and exergy benefit of nanofluid-based hybrid PV/T systems, in: Energy Conversion and Management, Elsevier Ltd, 2016, pp. 431–444.
[18] M. Ahmed, A. Radwan, in: Performance Evaluation of New Modified Low-Concentrator Polycrystalline Silicon Photovoltaic/thermal Systems, Energy Conversion and Management, 2017, pp. 593–607.
[19] K. Sopian, et al., in: Performance Analysis of Photovoltaic Thermal Air Heaters, Energy Conversion and Management, 1996.
[20] F. Yazdanifard, M. Ameri, E. Ebrahimnia-Bajestan, Performance of nanofluid-based photovoltaic/thermal systems: a review, in: Renewable and Sustainable Energy Reviews, 2017, pp. 323–352.
[21] M. Hemmat Esfe, M.H. Kamyab, M. Valadkhani, Application of nanofluids and fluids in photovoltaic thermal system: an updated review, in: Solar Energy, 2020.
[22] N. Aste, et al., Performance monitoring and modeling of an uncovered photovoltaic-thermal (PVT) water collector, in: Solar Energy, 2016, pp. 551–568.
[23] Y. Tripanagnostopoulos, Aspects and improvements of hybrid photovoltaic/thermal solar energy systems, in: Solar Energy, 2007, pp. 1117–1131.
[24] M. Lämmle, et al., Development and modelling of highly-efficient PVT collectors with low-emissivity coatings, in: Solar Energy, 2016.
[25] M. Lämmle, C. Thoma, M. Hermann, A PVT collector concept with variable film insulation and low-emissivity coating, in: Energy Procedia, 2016.
[26] M. Gonçalves, et al., A review of the challenges posed by the use of vacuum panels in external insulation finishing systems, Appl. Energy 257 (2020), 114028.
[27] S. Schiavoni, F. Bianchi, F. Asdrubali, Insulation materials for the building sector: a review and comparative analysis, Renew. Sustain. Energy Rev. 62 (2016) 988–1011.
[28] A. Uriarte, et al., Vacuum insulation panels in construction solutions for energy efficient retrofitting of buildings. Two case studies in Spain and Sweden, Energy Build. 197 (2019) 131–139.
[29] R. Baetens, et al., Vacuum insulation panels for building applications: a review and beyond, Energy Build. 42 (2) (2010) 147–172.
[30] T. Katsura, et al., Thermal performance analysis of a new structured-core translucent vacuum insulation panel in comparison to vacuum glazing: experimental and theoretically validated analyses, in: Solar Energy, 2020, pp. 326–346.
[31] R.W. Moss, et al., Performance and operational effectiveness of evacuated flat plate solar collectors compared with conventional thermal, PVT and PV panels, Appl. Energy 216 (2018) 588–601.
[32] S. Memon, P.C. Eames, Design and development of lead-free glass-metallic vacuum materials for the construction and thermal performance of smart fusion edge-sealed vacuum glazing, Energy Build. 227 (2020), 110430.
[33] A.E.M.A. Harb, et al., Influence of varying the Ethylene-Vinyl Acetate layer thicknesses on the performance of a polycrystalline silicon solar cell integrated with a microchannel heat sink, in: Solar Energy, 2020.
[34] Y. Fang, F. Arya, Evacuated glazing with tempered glass, Sol. Energy 183 (2019) 240–247.
[35] S. Memon, et al., A new low-temperature hermetic composite edge seal for the fabrication of triple vacuum glazing, Vacuum 120 (2015) 73–82.
[36] J.S. Jayakumar, et al., Experimental and CFD estimation of heat transfer in helically coiled heat exchangers, in: Chemical Engineering Research and Design, 2008, pp. 221–232.
[37] J. Zhou, et al., Temperature distribution of photovoltaic module based on finite element simulation, in: Solar Energy, 2015.
[38] F. Arya, et al., Vacuum enclosures for solar thermal panels Part 1: fabrication and hot-box testing, Sol. Energy 174 (2018) 1212–1223.
[39] J.-S. Kwon, et al., Effective thermal conductivity of various filling materials for vacuum insulation panels, Int. J. Heat Mass Tran. 52 (23–24) (2009) 5525–5532.
[40] A. Fluent, Ansys Fluent Theory Guide, vol. 15317, ANSYS Inc., USA, 2011, pp. 724–746.
[41] Z. Ling, et al., Review on thermal management systems using phase change materials for electronic components, Li-ion batteries and photovoltaic modules, in: Renewable and Sustainable Energy Reviews, 2014.
[42] M. Emam, M. Ahmed, Performance analysis of a new concentrator photovoltaic system integrated with phase change material and water jacket, Sol. Energy 173 (2018) 1158–1172.
[43] S. Park, et al., Energy and exergy analysis of typical renewable energy systems, Renew. Sustain. Energy Rev. 30 (2014) 105–123.
[44] G. Evola, L. Marletta, Exergy and thermoeconomic optimization of a water-cooled glazed hybrid photovoltaic/thermal (PVT) collector, in: Solar Energy, Elsevier Ltd, 2014, pp. 12–25.
[45] A. Hegazi, O. Abdelrehim, A. Khater, Parametric optimization of earth-air heat exchangers (EAHEs) for central air conditioning, Int. J. Refrig. 129 (2021) 278–289.
[46] A. Radwan, S. Ookawara, M. Ahmed, in: Thermal Management of Concentrator Photovoltaic Systems Using Two-phase Flow Boiling in Double-Layer Microchannel Heat Sinks, Applied Energy, 2019, pp. 404–419.
[47] A. Joshi, et al., Performance evaluation of a hybrid photovoltaic thermal (PV/T)(glass-to-glass) system, Int. J. Therm. Sci. 48 (1) (2009) 154–164.
[48] M.E.A. Slimani, et al., A detailed thermal-electrical model of three photovoltaic/thermal (PV/T) hybrid air collectors and photovoltaic (PV) module: comparative study under Algiers climatic conditions, Energy Convers. Manag. 133 (2017) 458–476.
[49] A. Radwan, et al., Development of a new vacuum-based photovoltaic/thermal collector{,} thermal and exergy analyses, in: Sustainable Energy Fuels, The Royal Society of Chemistry, 2020.
[50] A. Radwan, et al., Analysis of a vacuum-based photovoltaic thermal collector, in: Energy Reports, 2020, pp. 236–24242.